Dalton Transactions

ROYAL SOCIETY OF CHEMISTRY

PAPER

View Article Online
View Journal | View Issue

Cite this: *Dalton Trans.*, 2022, **51**, 5322

Clinically used antifungal azoles as ligands for gold(III) complexes: the influence of the Au(III) ion on the antimicrobial activity of the complex†

Nevena Lj. Stevanović, [a] Jakob Kljun, *[b] Ivana Aleksic, [c] Sanja Skaro Bogojevic, [c] Dusan Milivojevic, [c] Aleksandar Veselinovic, [d] Iztok Turel, *[b] Miloš I. Djuran, *[e] Jasmina Nikodinovic-Runic *[c] and Biljana Đ. Glišić *[a]

In a search for novel antimicrobial metal-based therapeutic agents, mononuclear gold(III) complexes **1–7** of the general formula [$AuCl_3$(azole)], where azole stands for imidazole (im, **1**), 1-isopropylimidazole (ipim, **2**), 1-phenylimidazole (phim, **3**), clotrimazole (ctz, **4**), econazole (ecz, **5**), tioconazole (tcz, **6**) and voriconazole (vcz, **7**) were synthesized, characterized and biologically evaluated. In all complexes, the corresponding azole ligand is monodentately coordinated to the Au(III) *via* the imidazole or triazole nitrogen atom, while the remaining coordination sites are occupied by chloride anions leading to the square-planar arrangement. *In vitro* antimicrobial assays showed that the complexation of inactive azoles, imidazole, 1-isopropylimidazole and 1-phenylimidazole, to the Au(III) ion led to complexes **1–3**, respectively, with moderate activity against the investigated strains and low cytotoxicity on the human normal lung fibroblast cell line (MRC-5). Moreover, gold(III) complexes **4–7** with clinically used antifungal agents clotrimazole, econazole, tioconazole and voriconazole, respectively, have, in most cases, enhanced antimicrobial effectiveness relative to the corresponding azoles, with the best improvement achieved after complexation of tioconazole (**6**) and voriconazole (**7**). The complexes **4–7** and the corresponding antifungal azoles inhibited the growth of dermatophyte *Microsporum canis* at 50 and 25 μg mL^{-1}. Gold(III) complexes **1–3** significantly reduced the amount of ergosterol in the cell membrane of *Candida albicans* at the subinhibitory concentration of 0.5 × MIC (minimal inhibitory concentration), while the corresponding imidazole ligands did not significantly affect the ergosterol content, indicating that the mechanism of action of the gold(III)–azole complexes is associated with inhibition of ergosterol biosynthesis. Finally, complexes **5** and **6** significantly reduced the production of pyocyanin, a virulence factor in *Pseudomonas aeruginosa* controlled by quorum sensing, and increased cell survival after exposure to this bacterium. These findings could be of importance for the development of novel gold(III)-based antivirulence therapeutic agents that attenuate virulence without pronounced effect on the growth of the pathogens, offering a lower risk for resistance development.

Received 9th February 2022,
Accepted 9th March 2022

DOI: 10.1039/d2dt00411a

rsc.li/dalton

Introduction

The use of metals and metal compounds in medicine is diverse and includes fundamental wide-reaching medical problems such as bacterial and fungal,[1,2] viral[3] and parasitic[4] infections. Besides that, metal-based drugs are used to treat cancer,[5] rheumatoid arthritis and other inflammatory diseases,[6] bipolar[7] and gastrointestinal[8] disorders. An important advantage of a medicinal use of metal complexes over organic drugs is that they have a versatile geometry, which may lead to a higher clinical success rate of metal complexes.[9] Additionally, metal complexes can have different modes of action, which are often impossible to achieve with organic

[a]*University of Kragujevac, Faculty of Science, Department of Chemistry, R. Domanovića 12, 34000 Kragujevac, Serbia. E-mail: biljana.glisic@pmf.kg.ac.rs*
[b]*Faculty of Chemistry and Chemical Technology, University of Ljubljana, Večna pot 113, SI-1000 Ljubljana, Slovenia. E-mail: Jakob.Kljun@fkkt.uni-lj.si, Iztok.Turel@fkkt.uni-lj.si*
[c]*Institute of Molecular Genetics and Genetic Engineering, University of Belgrade, Vojvode Stepe 444a, 11042 Belgrade, Serbia. E-mail: jasmina.nikodinovic@imgge.bg.ac.rs*
[d]*University of Niš, Faculty of Medicine, Department of Chemistry, Blvd. Dr Zorana Đinđića 81, 18108 Niš, Serbia*
[e]*Serbian Academy of Sciences and Arts, Knez Mihailova 35, 11000 Belgrade, Serbia. E-mail: milos.djuran@pmf.kg.ac.rs*

†Electronic supplementary information (ESI) available: Fig. S1–S15 and Tables S1 and S2. CCDC 2099556–2099558 and 2099560. For ESI and crystallographic data in CIF or other electronic format see DOI: 10.1039/d2dt00411a

drugs, such as ligand exchange or release, formation of reactive oxygen species (ROS), redox activation and depletion of essential substrates.[10]

The pharmacological properties of gold and its compounds have been known since antiquity,[11] and to date, gold compounds have been studied against the causative agents of various diseases, although they are currently used only for the treatment of rheumatoid arthritis.[6] Interest in the antimicrobial activity of gold(I) and gold(III) complexes dates back to the discovery of Robert Koch at the end of the 19th century, who found that potassium dicyanidoaurate(I), $K[Au(CN)_2]$, inhibited the growth of *Mycobacterium tuberculosis*, which is a causative agent of tuberculosis.[6] Subsequently, a large number of gold(I) and gold(III) complexes were synthesized and showed remarkable antimicrobial activity against various bacterial and fungal species.[1] Interestingly, auranofin, a gold(I) complex used to treat rheumatoid arthritis, also shows a good activity against a variety of medically important fungal pathogens.[12]

Disruption of the bacterial cell wall and cytosolic membrane in different bacterial strains induced by gold(I) complexes was postulated as a possible mechanism of their antibacterial action.[13] Based on the scanning electron microscope (SEM) measurements, as well as docking studies, it was suggested that these complexes strongly bind to both Lys and Dap-type peptidoglycan layers, which may be the reason for damage of the bacterial cell wall and increasing membrane permeability.[13,14] The observed selectivity of gold(I) complexes towards Gram-positive in respect to the Gram-negative bacterial strains was explained by the different construction of their cell membrane. While Gram-positive bacteria have only a single layer membrane, Gram-negative strains feature an inner and an outer membrane that also includes efflux transporters.[15] Furthermore, Schultz and co-workers[16] reported that the FDA-approved auranofin manifested potent bactericidal activity against Gram-positive pathogenic bacteria. It was found that this gold(I) complex inhibits an enzyme, thioredoxin reductase (TrxR), not targeted by other antibiotics. Also, this complex retains efficacy against many clinically relevant drug-resistant strains, including in a mouse model of infection. Similar potent inhibition of bacterial TrxR was also reported for gold(I) complexes with different N-heterocyclic carbene (NHC) ligands. Antibacterial screening of these complexes afforded a particular high activity against Gram-positive strains, reflecting their high dependence on an intact Trx/TrxR system.[17] In respect to the gold(I) complexes, so far only limited attention has been paid to the elucidation of the mode of antimicrobial action of gold(III) complexes. More recently, the mechanism of antibacterial activity of cyclometalated gold(III) C^N complex was investigated in *Bacillus subtilis*.[18] It was found that this complex is a fast acting bactericidal drug, which is effective on a range of Gram-positive bacterial strains, but does not cause significant tissue toxicity *ex vivo* in mouse liver precision-cut tissue slices. Moreover, the investigated organogold(III) complex rapidly decreases the energy levels of the cells, but does not have any effect on bacterial membrane permeability or membrane potential, neither on reactive oxygen species (ROS) production. This finding was different with respect to the antimicrobial gold(I) complexes, including auranofin.[18]

Nitrogen-containing aromatic heterocyclic ring systems (N-heterocycles) have attracted considerable attention as scaffolds for compounds used in many different pharmacological fields, ranging from vitamins and herbicides to antifungal, antibacterial and anticancer agents.[19,20] Among them, azoles are of particular importance as potent broad-spectrum agents used as first-line therapy for the treatment of many invasive fungal infections associated with significant morbidity and mortality worldwide.[21] To achieve fungicidal activity, azoles are known to interfere with ergosterol synthesis by inhibiting the enzyme lanosterol 14α-demethylase.[22,23] However, enzyme inhibition by azoles is not exclusive to fungal cells and a wide range of significant toxicities has been observed for this class of agents, including hepatotoxicity, hallucinations and irregular cardiac function.[24] In addition, the use of azoles has been limited by the development and increase of primary and acquired resistance in fungal species.[25]

Despite the success of various metal-based drugs and antifungal azoles in medicine, there is undoubtedly still a need for the development of new agents to either treat incurable conditions or improve currently available treatments that lead to severe toxic side effects or development of resistance. To achieve this, our strategy is to the conjugate different azoles, including FDA-approved antifungals, with the biologically relevant Au(III) ion. This conjugation could increase the selectivity of a complex for intercellular/intracellular targets and contribute to overcome the typical mechanisms of drug resistance and improve the biological activity of the parent organic compound.[26] In view of this, seven mononuclear gold(III) complexes **1–7** of the general formula $[AuCl_3(azole)]$, where azole is imidazole (im, **1**), 1-isopropylimidazole (ipim, **2**), 1-phenylimidazole (phim, **3**), clotrimazole (ctz, **4**), econazole (ecz, **5**), tioconazole (tcz, **6**) and voriconazole (vcz, **7**) were synthesized and structurally characterized. They were also extensively studied for their antimicrobial and antiproliferative properties, including their effect on ergosterol biosynthesis in fungi and quorum sensing in bacteria. The influence of the coordinated Au(III) ion on the antimicrobial potential of the investigated complexes **1–7** was determined by comparing the antimicrobial activity of these complexes with that of the uncoordinated inactive and antifungally active respective azoles.

Results and discussion

Synthesis and structural characterization of gold(III) complexes 1–7

Antimicrobially inactive imidazole (im) and its two derivatives, 1-isopropylimidazole (ipim) and 1-phenylimidazole (phim) (Scheme 1a), are used for complexation with gold(III) and corresponding complexes $[AuCl_3(im)]$ (**1**), $[AuCl_3(ipim)]$ (**2**) and $[AuCl_3(phim)]$ (**3**) were used as model compounds for the synthesis and structural characterization of analogous gold(III)

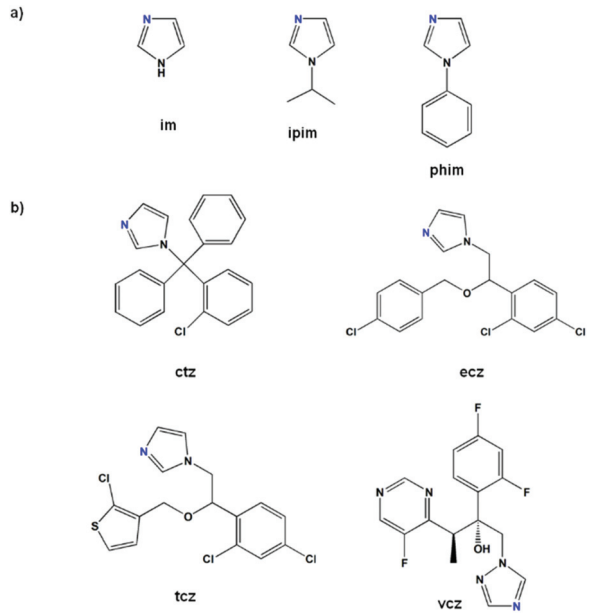

Scheme 1 Structural formula of imidazoles (imidazole, im; 1-isopropylimidazole, ipim; and 1-phenylimidazole, phim) (a) and antifungal azoles (clotrimazole, ctz; econazole, ecz; tioconazole, tcz; and voriconazole, vcz) (b) used as ligands for the synthesis of gold(III) complexes **1–7**, respectively. The nitrogen atoms included in Au(III) coordination are highlighted in blue.

complexes, [$AuCl_3$(ctz)] (**4**), [$AuCl_3$(ecz)] (**5**) [$AuCl_3$(tcz)] (**6**) and [$AuCl_3$(vcz)] (**7**), containing clinically used antifungal azoles, clotrimazole (ctz), econazole (ecz), tioconazole (tcz) and voriconazole (vcz) (Scheme 1b). To determine the influence of the coordinated Au(III) ion on the antimicrobial activity of complexes **1–7**, the biological properties of these complexes were compared with that of the uncoordinated inactive and antifungally active azoles. Complexes **1–7** were obtained by reacting equimolar amounts of K[$AuCl_4$] and the corresponding azole ligand in ethanol under reflux for 3 h. All complexes were characterized by CHN elemental microanalysis, high-resolution mass spectrometry, ^{1}H NMR, IR and UV-Vis spectroscopies, and molar conductivity measurements. The molecular structures of complexes **3–5** and **7** were determined by single crystal X-ray diffraction analysis.

Description of the single crystal structures. The molecular structures of complexes **3–5** and **7** are shown in Fig. 1, while the selected bond distances and structural parameters are listed in Table 1. The crystal structures of complexes **3**, **5** and **7** are new, while the crystal structure of the clotrimazole complex **4** was previously reported by Sánchez-Delgado *et al.*[27] While azole antifungals have been used in clinical practice for decades, there is surprisingly little structural data on their metal complexes. The most studied and structurally simplest antifungal azole – clotrimazole – is present in 19 structures of metal complexes in the Cambridge Structural Database (CSD; as of 10.2.2022, version 2021.3). Voriconazole has the most diverse chemistry due to the abundance of possible coordinat-

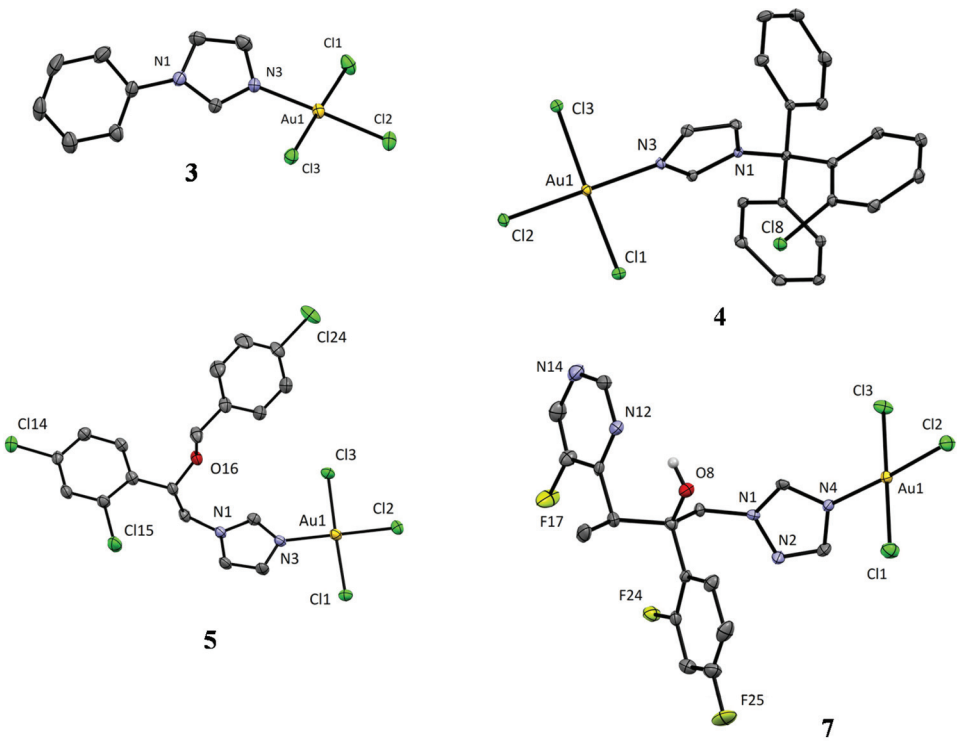

Fig. 1 Crystal structures of [$AuCl_3$(azole)] complexes, azole stands for 1-phenylimidazole (**3**), clotrimazole (**4**), econazole (**5**) and voriconazole (**7**). Thermal ellipsoids are drawn at 35% probability level. Hydrogen atoms bound to carbon atoms are omitted for better clarity.

Table 1 Bond lengths and selected structural parameters in gold(III) complexes **3–5** and **7**

Complex	**3**	**4**	**5**	**7**
Au–$N_{(azole)}$ (Å)	2.036(4)	2.019(3)	2.037(4)	2.009(6)
Au–$Cl_{(trans\text{-}N)}$ (Å)	2.262(1)	2.253(1)	2.262(1)	2.257(2)
Au–$Cl_{(cis\text{-}N)}$ (Å)	2.272(1)	2.279(1)	2.278(1)	2.279(2)
	2.283(1)	2.282(1)	2.275(1)	2.270(2)
τ_4/τ'_4	0.03/0.02	0.02/0.02	0.03/0.03	0.06/0.05
φ (°)	24.10	60.96	21.48	57.18

φ = angle between planes defined by the $AuCl_3N$ atoms and 5 atoms of the bound azole ring.

ing groups (4 × N, 1 × O) which can result in monodentate, polydentate and bridging binding modes to form both isolated and polymeric products. Currently, there are 9 structures reported in the CSD. And finally, for econazole, we report the first ever crystal structure of a metal complex.

All crystal structures show a square-planar geometry around the Au(III) ion (Fig. 1) with the maximum τ_4/τ'_4 values of 0.06/0.05 in the case of complex **7** (value 0 for square-planar and 1 for tetrahedral geometry).[28] The bond lengths are consistent with those reported in the CSD database. The Au–Cl bond is slightly shorter in the case of the chlorido ligand in *trans* position to the azole ligand in comparison with the *cis* chlorido ligands (2.25–2.26 *vs.* 2.27–2.28 Å), which is consistent with the more intense *trans* effect of the chlorido ligands (Table 1). An interesting detail in the coordination mode of the azole ligands is the dihedral angle φ between the $AuCl_3N$ plane and the plane defined by the 5 atoms of the coordinated azole ring (Table 1).

The crystal structures of **3** and **5** show a near coplanarity of the two planes with angles of approx. 20°, while dihedral angle values in the complexes **4** and **7** approach 60°. The latter is in better agreement with the reported data, which are, however, relatively scarce. The CSD database shows 12 hits for the substructure fragment $AuCl_3$(azole), where 'azole' stands for any 5-membered heterocycle bound to Au(III) through a nitrogen atom. In general, two types of complexes were differentiated. Those in which the azole ligand possesses an additional chelating group (O atoms in guanine derivatives, pendant N-heterocycles, or Schiff base imine nitrogens in bipy-type chelators; 7 structures in all) generally bind at an approx. 90° angle leading to a [4 + 1] gold coordination with a pseudo-square-pyramidal geometry. For the remaining structures, the dihedral angle values are about 60°. Since the structures of **3** and **5** do not show any obvious strong inter- or intramolecular interactions (except for the intramolecular hydrogen bond $O–H\cdots N_{(pyrimidine)}$), it is not possible at this stage to draw any conclusions (even speculative) to explain the cause-effect of the different bonding conformations of the azole ligands.

Spectroscopic characterization. The IR spectroscopic data for gold(III) complexes **1–7** are given in the Experimental section and agree with the structures determined by X-ray diffraction analysis (for complexes **3–5** and **7**). Thus several distinguishable bands in the wavelength region of 4000–450 cm^{-1} were observed in IR spectra of the investigated gold(III) complexes. Accordingly, the bands at ~3100–3000 cm^{-1} can be attributed to the aromatic C–H stretching vibrations, while the bands at ~2900 cm^{-1} reveal the existence of the $C_{aliphatic}$–H bonds. All the complexes show characteristic vibrations of the aromatic rings (both six- and five-membered), ($\nu(C_{ar}{=}C_{ar})$ and $\nu(C_{ar}{=}N)$), in the 1636–1373 cm^{-1} region, confirming the coordination of the corresponding azole.[29,30] Moreover, in the spectrum of tcz complex **6**, a band at 748 cm^{-1} was detected due to the ν(C–S),[30] while complex **7** exhibits a broad absorption at 3436 cm^{-1}, due to the O–H stretching vibration of voriconazole.

The molar conductivities measured immediately after dissolving the complexes **1–7** in DMF given in the Experimental section are in accordance with their non-electrolytic nature.[31,32]

The UV-Vis spectra of gold(III) complexes **1–7** and the corresponding ligands were recorded in chloroform. The absorption maxima (λ_{max}) for the complexes (λ_{max} = 260, 315, 299, 301, 300, 301 and 305 nm for **1–7**, respectively) are due to the LMCT (ligand-to-metal charge transfer) transitions.[33–35] Moreover, the absorbance peaks of complexes **1–7** show significant red shifts compared to those of the free ligands (λ_{max} ~ 260 nm for the azoles). The UV–Vis stability of gold(III) complexes **1–7** was studied during 48 h in DMSO solution in the dark at room temperature. The intensity of the absorption maxima of these complexes decreased slightly during 48 h (up to 11% for complex **3**) compared with those recorded immediately after dissolution of the complexes. Nevertheless, in all cases the shape of the spectra and the position of the absorption maxima of **1–7** remained unchanged during the time studied which is consistent with their stability in solution (for the stability of **7** see Fig. S1†). Fig. S1† also illustrates the UV-Vis spectra of the corresponding voriconazole ligand recorded in DMSO at room temperature.

The ^{1}H NMR spectra of gold(III) complexes were recorded in DMSO-d_6 for **1–3** and their respective ligands (im, ipim and phim) and in $CDCl_3$ for **4–7** and the corresponding azole ligands (ctz, ecz, tcz and vcz) (Fig. S2–S8†). All these spectra were assigned based on previous assignments of the corresponding ^{1}H NMR spectra of azoles measured in different solvents.[29,30,36–38] The corresponding spectroscopic data for the selected azoles are given in ESI.† The ^{1}H NMR spectra of the gold(III) complexes **1–7** were different from those of the uncoordinated azoles. Auration of all azoles resulted in ^{1}H deshielding, as a consequence of the strong electron-withdrawing effect of Au(III) ion.[39] In all cases, the largest chemical shifts were observed for the protons adjacent to the nitrogen binding atom, *i.e.* C4H for **1** ($\Delta\delta$ = +0.48 ppm), C2H proton for complexes **2–6** (up to $\Delta\delta$ = +1.00 ppm for **2**), while for the triazole-containing complex **7**, the largest shift was observed for proton C5H ($\Delta\delta$ = +0.77 ppm) (Fig. S2–S8†).

The positive ion ESI mass spectra for gold(III) complexes **1–7** were in agreement with the patterns simulated for the corresponding molecular cations, confirming their composition.

Evaluation of biological activities of the gold(III) complexes 1–7

Antifungal activity. The antifungal properties of azoles have been studied from the late 1970s, and they found their way into clinics.[40] Here, we assessed the effects of the complexation of three inactive (im, ipim and phim) model azole ligands and four antifungally active azoles (ctz, ecz, tcz and vcz) with Au(III) ion on their *in vitro* antifungal properties (Table 2). The activity of $K[AuCl_4]$, a gold(III) salt used for the synthesis of the complexes **1–7**, against *C. albicans* and *C. parapsilosis*, was investigated previously and MIC values were found to be 100 and 200 μM, respectively.[41] In the present study, our selection of five *Candida* strains included *C. auris*, an emerging multi-drug-resistant yeast, that causes invasive healthcare-associated infections with high mortality worldwide.[42] In addition, *Microsporum canis* isolated from a canine skin swab was included in the antifungal evaluation of the complexes and corresponding azole ligands. *M. canis* is a common zoophilic dermatophyte that causes clinical conditions in many animal species, including humans which are often characterized by multifocal alopecia, scaling and circular lesions.[43] Given that dermatophytoses are highly prevalent worldwide (20–25%) and are characterized by relapses and treatment failures,[44,45] new treatment options are highly sought after.

Overall, all gold(III) complexes **1–7** showed anti-*Candida* activity with MIC values ranging from 0.2–484 μM (0.1–200 μg mL^{-1}), while some of the azoles (im, ipim and phim) were completely inactive at the maximum concentrations tested (1.3–3 mM; 200 μg mL^{-1}). These three azoles also showed lower cytotoxicity compared to the gold(III) complexes **1–7** and the clinically used ctz, ecz, tcz and vcz azoles. In the case of the azoles, which are established anti-*Candida* compounds, the presence of the coordinated Au(III) ion generally increased the activity of the corresponding complexes **4–7**, with the best improvement achieved for complexes **4**, **6** and **7**. This improvement in activity of the gold(III) complexes also differs between microorganisms. The charts presenting the difference in the activity (1/MIC, μM) on the type of the tested fungal strains between gold(III) complex and corresponding azole ligand were given in Fig. S9 and S10.† The strain *C. glabrata* was most affected by gold(III) complexes **5–7**, with a 6.1- to 7.5-fold improvement in activity compared with the uncoordinated ecz, tcz and vcz ligands, respectively (μM concentrations; Table 2). Complexes **4** and **6** showed a 45-fold and 21.4-fold increase (μM) in activity against *C. krusei.* The highest increase in activity against *C. auris* strain of almost 30-fold (μM) was observed with complex **7**. It is known that *C. auris* is highly resistant to azoles,[42,46,47] which is probably due to its phylogenetic relationship with other *Candida* species, which are inherently resistant to several antifungals. Therefore, the observed increase in activity with complex **7** is of great importance and could serve as a lead for further optimization.

Of the gold(III) complexes **1–3** with antifungally inactive azole ligands, complex **3** was the most cytotoxic, whereas **4** and **6**, containing ctz and tcz, respectively, showed pronounced cytotoxicity of the gold(III) complexes with antifungal azoles (Table 2). The selectivity index (SI) as the gap between cytotoxicity and antimicrobial activity was determined for gold(III) complexes **1–7** and the corresponding azoles by dividing the given IC_{50} value by the obtained MIC value (Table S1†). The SI values calculated for the complexes ranged from particularly high 1075 (complex **7**/*C. parapsilosis*) to less favourable 0.3

Table 2 Antifungal activity of gold(III) complexes **1–7** and the corresponding azoles against the selection of Candida strains (MIC, μM and μg mL^{-1}) in comparison to their antiproliferative effect on healthy human fibroblast MRC-5 cell line (IC_{50}, μM and μg mL^{-1})[a]

Test organism	*C. albicans*[b]		*C. parapsilosis*[b]		*C. glabrata*		*C. krusei*		*C. auris*			
	ATCC 10231		ATCC 22019		ATCC 2001		ATCC 6258		ATCC 21092		MRC-5	
Au(III) complex/azole	μM	μg mL^{-1}	μM	μg mL^{-1}	μM	μg mL^{-1}	μM	μg mL^{-1}	μM	μg mL^{-1}	μM	μg mL^{-1}
Au(III) complex/imidazole												
$[AuCl_3(im)]$ (**1**)	135	50	135	50	135	50	67.5	25	270	100	310	115
Imidazole (im)	>2938	>200	>2938	>200	>2938	>200	>2938	>200	>2938	>200	>2938	>200
$[AuCl_3(ipim)]$ (**2**)	242	100	242	100	484	200	242	100	242	100	145	60
1-Isopropylimidazole (ipim)	>1815	>200	>1815	>200	>1815	>200	>1815	>200	>1815	>200	>1815	>200
$[AuCl_3(phim)]$ (**3**)	112	50	112	50	112	50	112	50	56	25	89	40
1-Phenylimidazole (phim)	>1387	>200	1387	200	1387	200	1387	200	>1387	>200	1387	200
Au(III) complex/clinically used azole												
$[AuCl_3(ctz)]$ (**4**)	38.6	25	**1.4**	0.9	4.8	3.1	0.4	0.3	**1.9**	1.2	6.2	4
Clotrimazole (ctz)	2.6	0.9	10.2	3.5	9.1	3.2	1.4	0.5	9.1	3.2	8.7	3
$[AuCl_3(ecz)]$ (**5**)	4.6	3.1	2.5	1.7	**9.1**	6.2	18.3	12.5	9.1	6.2	26.3	18
Econazole (ecz)	7.0	2.7	3.9	1.5	56.2	21.5	14.1	5.4	7.0	2.7	10.1	3.9
$[AuCl_3(tcz)]$ (**6**)	0.6	0.4	0.6	0.4	**9.0**	**6.2**	**1.5**	**1**	3.6	2.5	6.5	4.5
Tioconazole (tcz)	2.3	0.9	0.3	0.1	64.5	25	32.2	12.5	8.1	3.1	14.2	5.5
$[AuCl_3(vcz)]$ (**7**)	**4.8**[c]	**3.1**	0.2	0.1	**76.6**	**50**	1.5	1	**19.1**	**12.5**	215	140
Voriconazole (vcz)	35.8	12.5	0.3	0.1	572	200	1.4	0.5	572	200	859	300

[a] Standard deviation values were between 0–2%. [b] MIC values of $K[AuCl_4]$ against *C. albicans* and *C. parapsilosis* were found to be 100 and 200 μM (37.78 and 75.58 μg mL^{-1}), respectively.[41] [c] Bold and underlined are values that are ≥4-fold improved in comparison to the corresponding clinically used antifungals.

(complex **2**/*C. glabrata*). These calculations agree with the SI values of the corresponding azoles, with imidazole being non-toxic at concentrations tested, and voriconazole having the SI value of 2863 on *C. parapsilosis*.

The complexes and the corresponding azole ligands were tested against *M. canis* at two concentrations, 50 and 25 μg mL^{-1} (Fig. S11†). In the experiment with the higher concentration, complete inhibition of fungal growth was observed after 7 days in wells with complexes **4–7**, while delayed growth was observed in the wells with complex **3** compared to control. However, the corresponding azoles also showed comparable activity.

Previous antimicrobial studies on gold(III) complexes showed good antibacterial activity, but moderate antifungal activity,[1,48] which can be attributed to the choice of the ligands. On the other hand, azole derivatives containing coordinated Au(III) ions were also investigated for their anticancer therapeutic applications.[49]

Effect on the ergosterol biosynthesis. Considering that clinically used antifungal azoles inhibit cytochrome P450 involved in ergosterol biosynthesis[50] evidenced by lower levels of ergosterol in strains grown in the presence of subinhibitory concentrations of azoles,[51] ergosterol levels in *C. albicans* treated with complexes **1–3** and the corresponding azoles im, ipim and phim were assessed, as these compounds have not been used as antifungal azoles. Complexes **1–3** significantly reduced ergosterol levels at a concentration of 0.5 × MIC (Fig. 2). Of the non-antifungal azoles, only phim slightly reduced ergosterol levels at a concentration of 0.5 × MIC, while im and ipim did not change the ergosterol content compared to the untreated control. This suggests that part of the mechanism of action of gold(III)–azole complexes **1–3** is the inhibition of ergosterol biosynthesis or the interaction with sterol itself[52] due to the presence of the Au(III) ion within structure.

Antibacterial properties of complexes 1–7. Azoles, and among them triazoles in particular, are usually tested as antifungals. However, following the general trend of drug repurposing, their antibacterial properties were also investigated in this study (Table 3). The antibacterial activity of complexes **1–7** and the corresponding uncoordinated azoles is lower than that of antifungal activity (Table 2), but still some interesting patterns were observed. As was mentioned, the moderate activity of $K[AuCl_4]$ against different bacterial species was observed previously.[41]

The uncoordinated model azole ligands im, ipim and phim had no detectable effect on the growth of the bacterial strains tested (Table 3). Likewise, the antifungal azoles ctz, ecz, tcz and vcz showed moderate to good activity only against *S. aureus* strains (MIC 14–570 μM; 5.4–200 μg mL^{-1}). Interestingly, *S. aureus* MRSA was the most sensitive, with MIC of 14.1 and 32.2 μM (5.4 and 12.5 μg mL^{-1}) for ecz and tcz, respectively. Previously, ctz, ecz and tcz were shown to affect the growth of *Staphylococcus* strains[53–56] and some Gram-negative bacterial species, however there are no available data on the antibacterial activity of their metal complexes. Complexation of the investigated azoles with Au(III) ion resulted in the emergence of the activity against other bacterial strains such as *E. coli*, with the lowest MIC of 30.9 μM (20 μg mL^{-1}) for complex **4**. Complex **5** showed a MIC of 18.3 μM (12.5 μg mL^{-1}) against *S. aureus* ATCC 259233 (Table 3). Complexes **5** and **6** showed good activity against *P. aeruginosa* PA14 with MIC of 18.3 and 18.1 μM, respectively (12.5 μg mL^{-1}). The overall improvement in antibacterial activity when comparing gold(III) complexes **1–7** with the corresponding azole ligands is more pronounced in comparison to antifungal activity, as an actual gain in activity was observed in most cases. This can be also seen in Fig. S12 and S13,† which illustrate the difference in the activity (1/MIC, μM) between gold(III)–azole complex and the corresponding azole ligand on the type of the tested bacterial strains. Even with azoles that initially showed some antibacterial activity, as in the case of complex **4**, a 30.2-fold improvement (μM concentrations) of activity was detected in comparison to ctz against *S. aureus* NCTC 6571.

Previously, Khabnadideh *et al.* reported the synthesis of *N*-alkylated imidazole derivatives as antibacterial agents tested on *P. aeruginosa*, *E. coli* and *S. aureus*, where the lowest MIC of 10 μg mL^{-1} was obtained in *S. aureus* for nonylimidazole.[57] Phenylimidazole and the gold(III) complex **3** showed moderate activity against *E. coli* and two *S. aureus* strains (Table 3). Similarly, phenylimidazole was previously used as a scaffold for more complex derivatives, which gained moderate antimicrobial potential against *E. coli* and *S. aureus*[58,59] compared to norfloxacin (zones of inhibition were measured).

Savić *et al.* in a comparative antimicrobial study[48] reported a series of gold(III) complexes with aromatic nitrogen-containing heterocycles, finding that *P. aeruginosa* was the most sensitive to the tested compounds. We have also reported dinuclear gold(III) complexes with bridging aromatic nitrogen-containing heterocyclic ligands and studied their antimicrobial activities,[60] where the MIC values for *E. coli* and *P. aeruginosa* were comparable to the results observed in this study. Significant antibacterial activity against *B. subtilis* and *S. aureus* strains was also previously observed for organogold(III) complex with a bidentate C^N scaffold, which was found to cause a decrease

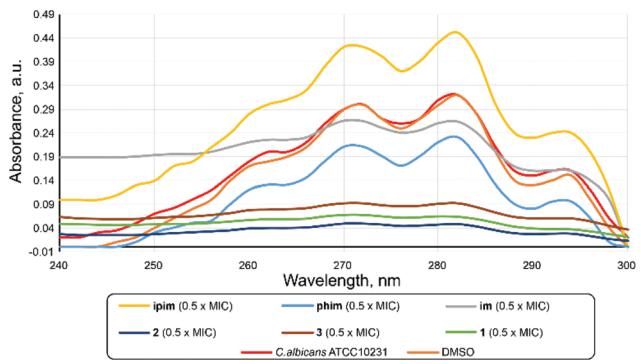

Fig. 2 UV-Vis spectrophotometric ergosterol profiles between 240 and 300 nm of *C. albicans* ATCC 10231 cultures treated with 0.5 × MIC concentrations of azoles im, ipim and phim, and corresponding complexes **1–3**.

Table 3 Minimum inhibitory concentrations (MIC, μM and μg mL^{-1}) of the gold(III) complexes **1–7** and corresponding uncoordinated azoles against bacterial strains[a,b]

Test organism	*E. coli* NCTC 9001		*P. aeruginosa* NCTC 10332		*P. aeruginosa* PA14		*P. aeruginosa* BK25H		*S. aureus* ATCC 259233		*S. aureus* NCTC6571		*S. aureus* MRSA	
Au(III) complex/azole	μM	μg mL^{-1}	μM	μg mL^{-1}	μM	μg mL^{-1}	μM	μg mL^{-1}	μM	μg mL^{-1}	μM	μg mL^{-1}	μM	μg mL^{-1}
Au(III) complex/imidazole														
[$AuCl_3$(im)] (**1**)	67.5	25	135	50	67.5	25	270	100	67.5	25	135	50	67.5	25
Imidazole (im)	>2938	>200	>2938	>200	>2938	>200	>2938	>200	>2938	>200	>2938	>200	>2938	>200
[$AuCl_3$(ipim)] (**2**)	60.5	25	121	50	121	50	121	50	60.5	25	121	50	60.5	25
1-Isopropylimidazole (ipim)	>1815	>200	>1815	>200	>1815	>200	>1815	>200	>1815	>200	>1815	>200	>1815	>200
[$AuCl_3$(phim)] (**3**)	55.9	25	223	100	223	50	112	50	55.9	25	56.0	25	27.9	12.5
1-Phenylimidazole (phim)	1387	>200	1387	>200	1387	>200	1387	>200	1387	>200	1387	>200	1387	>200
Au(III) complex/clinically used azole														
[$AuCl_3$(ctz)] (**4**)	30.9	20	231	150	38.6	25	38.6	100	19.3	12.5	9.6	6.2	19.3	12.5
Clotrimazole (ctz)	>580	>200	>580	>200	>580	>200	>580	>200	290	100	290	100	36.3	12.5
[$AuCl_3$(ecz)] (**5**)	36.5	25	219	150	18.3	12.5	18.3	50	18.3	12.5	36.5	25	9.1	6.2
Econazole (ecz)	>450	>172	>450	>172	>450	>172	>450	>172	225	86	28.1	10.7	14.1	5.4
[$AuCl_3$(tcz)] (**6**)	36.2	25	217	150	18.1	12.5	18.1	50	72.4	50	36.2	25	18.1	12.5
Tioconazole (tcz)	>516	>200	>516	>200	>516	>200	>516	>200	258	100	129	50	32.2	12.5
[$AuCl_3$(vcz)] (**7**)	76.6	50	268	175	76.6	50	76.6	50	153	100	153	100	76.6	50
Voriconazole (vcz)	572	200	572	200	572	200	572	200	572	200	572	200	572	200

[a] Standard deviation values were between 0–2%. [b] The moderate activity of K[$AuCl_4$] against different bacterial species was observed previously.[41]

of the energy levels of the *B. subtilis* cells, without any effect on bacterial membrane permeability or membrane potential, or on the ROS generation.[18]

Anti-quorum sensing properties of the investigated azoles and their complexes 1–7: effects on pyocyanin, violacein, and prodigiosin production. Quorum sensing (QS) is a bacterial cell – cell communication process that involves the production, detection, and response to extracellular signalling molecules.[61] In recent years, many QS-systems were evaluated as targets for antivirulence therapy, indicating the possibility of reducing pathogenicity of tested microorganisms and easier eradication when co-treated with antibiotics.[62,63] Thus, numerous compounds, both natural and synthetic, have been examined in this context.[64] In this study, the quorum sensing inhibitory potential of the selected azoles and the corresponding gold(III) complexes **1–7** was tested using different biosensor strains: *Pseudomonas aeruginosa* PA14 (pyocyanin producer), *Chromobacterium violaceum* CV026 (violacein producer) and *Serratia marcescens* (prodigiosin producer).

Pyocyanin is a bacterial pigment, whose production is controlled by the quorum sensing process and it causes multiple deleterious effects on mammalian cells, such as inhibition of cell respiration, disruption of calcium homeostasis and inactivation of catalase.[65] To examine whether the tested compound has a specific potential to inhibit the production of pyocyanin, subinhibitory concentrations of all compounds were used in the assay with *P. aeruginosa* PA14, to investigate their potential to interfere with the quorum sensing process that occurs in a high bacterial population. All gold(III)–azole complexes showed inhibition of pyocyanin production between 80 and 50%, compared to the untreated control when tested at a concentration of 20 μg mL^{-1} (Fig. 3a). Apart from ecz and tcz, the other investigated azoles showed no detectable activity at this concentration. Complexes **5** and **6** were the most potent inhibitors of pyocyanin production and were active even at lower concentrations (Fig. 3b). The lack of blue/green redox-active pigment was evident in the supernatants of the *P. aeruginosa* PA14 culture (Fig. 3c). The 4- and 8-fold improvement in activity was observed in the case of **5** and **6** compared to the corresponding uncoordinated azoles at 10 μg mL^{-1}. This improvement was consistent even at concentrations as low as 5 μg mL^{-1} (Fig. 3b).

To further test if this anti-QS activity can be used in the development of anti-infective molecules, an *in vitro* assay was performed using A549 human cancer cells to evaluate the ability of the compounds to prevent *P. aeruginosa* from killing the cells. The *P. aeruginosa* BK25H strain used in this experiment was described in our previous work.[66] This strain was a particularly good producer of pyocyanin and caused death of approximately 55% of the cells in *in vitro* assay with A549 cells. Complexes **5** and **6** were used at subinhibitory and subtoxic concentrations (Tables 2 and 3) because of their strong potential to inhibit production of pyocyanin in the *P. aeruginosa* PA14 strain (Fig. 3). Both compounds decreased cell death in the presence of *P. aeruginosa* BK25H by approximately 15% at a concentration of 5 μg mL^{-1} (7.3 and 7.2 μM for **5** and **6**, respectively). Complex **6** showed similar activity even at a concentration of 2.5 μg mL^{-1} (3.6 μM; Fig. 4). The corresponding azoles (ecz and tcz) were not able to modulate the cell death caused by *P. aeruginosa* BK25H, with exception of tcz at 5 μg mL^{-1} (12.9 μM; Fig. 4).

Although significant activity of gold(III) complexes on pyocyanin production was observed (Fig. 3), these compounds did

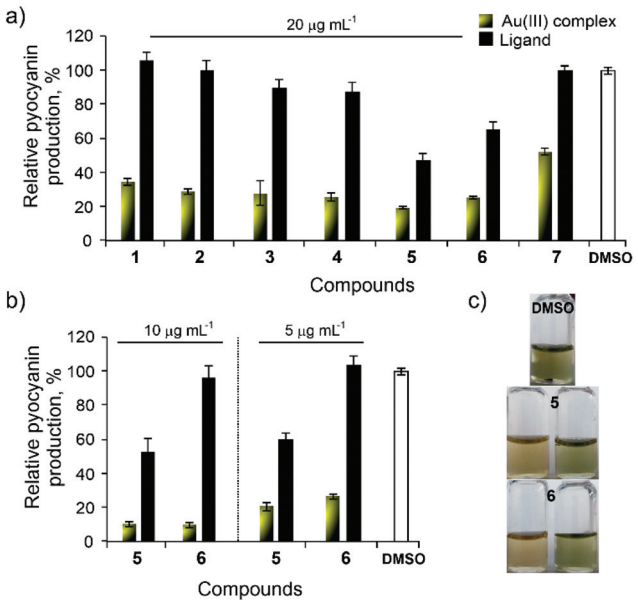

Fig. 3 Relative pyocyanin production by *Pseudomonas aeruginosa* PA14 strain in the presence of complexes **1–7** and the corresponding azoles at a concentration of 20 μg mL^{-1} (a), and at lower concentrations of 10 and 5 μg mL^{-1} (b). Appearance of the culture supernatants upon treatment with DMSO and complexes **5** and **6** at 10 μg mL^{-1} (c).

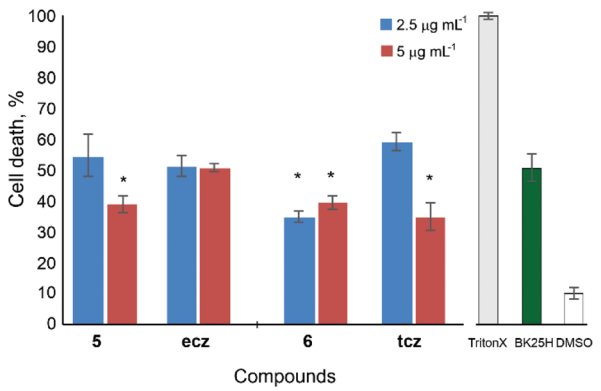

Fig. 4 Relative cell death caused by *P. aeruginosa* BK25H in the presence of complexes **5** and **6** and their corresponding azoles ecz and tcz at concentrations of 2.5 and 5 μg mL^{-1} (* = $p < 0.05$).

not modulate the biosynthesis of violacein and prodigiosin to the same extent. Both pigments are also under the control of the QS network.

Moderate to low activity was observed at a concentration of 200 μg per disc for complexes **5** and **7**, and phim azole on violacein production, while **1–3** and **6** induced growth inhibition of this strain under tested conditions (Fig. S14†). Complex **7** and phim also affected prodigiosin biosynthesis in *S. marcescens*, while **2**, **3** and **7** showed some growth inhibition of this strain as well (Fig. S15†). Non-antifungal azole phim showed moderate activity on the production of both pigments, while other investigated azoles had no effect. The lower activity on the production of violacein and prodigiosin could be explained by the different QS pathways of *C. violaceum* and *S. marcescens*. These two strains do not possess the *Pseudomonas* quinolone signalling system (PQS), specific only to *P. aeruginosa*, which in combination with Las and RhL regulates pyocyanin production.[67] Previously, nickel(II) complexes with imidazoles were tested for their ability to inhibit pyocyanin production in pathogenic strains isolated from cystic fibrosis patients, and these complexes showed no effect.[68] 2-Aminobenzimidazole derivatives have been reported as compounds with the potential to interfere with the QS process of *P. aeruginosa* and to inhibit biofilm formation.[69] Azole compounds have not been sufficiently studied as quorum quenchers.

Experimental

Materials and measurements

Potassium tetrachloridoaurate(III) (K[AuCl$_4$]), imidazole (im), 1-isopropylimidazole (ipim), 1-phenylimidazole (phim), clotrimazole (ctz), econazole (ecz), tioconazole (tcz), voriconazole (vcz), ethanol, chloroform, dimethylformamide (DMF), acetone, deuterated dimethyl sulfoxide (DMSO-d_6) and chloroform ($CDCl_3$) were obtained from commercial suppliers (Sigma-Aldrich, Acros Organics and Euroisotop). All chemicals were of analytical grade and used without further purification. Solvents were used as received.

Elemental microanalyses of the synthesized gold(III)–azole complexes **1–7** for carbon, hydrogen and nitrogen were performed using a PerkinElmer 2400 Series II instrument (CHN). The ESI-HRMS spectra in the positive mode were recorded after dissolving the corresponding complex in CH_3CN with an Agilent 62224 accurate mass spectrometer, using time of flight liquid chromatography/mass spectrometry. The IR spectra were recorded on a Bruker FTIR Alpha Platinum ATR spectrometer over the wavenumber range 4000–400 cm^{-1}. The UV-Vis spectra were recorded over the wavelength range of 500–200 nm on a PerkinElmer Lambda 750 UV/Vis/near-IR spectrophotometer after dissolving of the gold(III) complexes **1–7** in $CHCl_3$. The concentration of the solutions used for these measurements was 3.2×10^{-4} M. UV-Vis stability measurements were performed on a Shimadzu double-beam spectrophotometer after dissolving the gold(III) complexes **1–7** in DMSO immediately after their dissolution, as well as after 24 and 48 h standing at room temperature, over the wavelength range of 500–200 nm. The concentration of the solutions used for these measurements was 1.7×10^{-4} M (**1**), 2.7×10^{-4} M (**2**, **3** and **7**), 1.8×10^{-4} M (**4**), 2.0×10^{-4} M (**5**) and 2.3×10^{-4} M (**6**). The ^{1}H NMR spectra of gold(III) complexes **1–3** were recorded on a Varian Gemini 2000 spectrometer at 200 MHz, while those of gold(III)–azole complexes **4–7** were recorded on a Bruker Avance III spectrometer at 500 MHz at room temperature with tetramethylsilane as the internal standard. 5.0 mg of each compound was dissolved in 0.6 mL of DMSO for **1–3** or $CDCl_3$ for **4–7** and transferred into a 5 mm NMR tube.

Chemical shifts, σ, are expressed in ppm (parts per million) and scalar couplings, J, are reported in Hz (Hertz). The splitting of protons is designated as: s, singlet; d, doublet; dd, doublet of doublets; t, triplet; td, triplet of doublets; q, quartet and m, multiplet. Molar conductance measurements were carried out at room temperature using HI-2003 Edge® Conductivity Meter, with the concentration of the solutions of gold(III)–azole complexes in DMF being 1×10^{-3} M. For X-ray structural analysis, single crystals of complexes were surrounded with silicon grease, mounted onto the tip of glass fibres and transferred to the goniometer head in the liquid nitrogen cryostream (150(2) K). Data were collected on a SuperNova diffractometer equipped with Atlas detector using CrysAlis software with monochromated Mo Kα (0.71073 Å).[70] The initial structural models were obtained *via* direct methods using Olex2 graphical user interface[71] implemented in SHELXT. A full-matrix least-squares refinement on F^2 magnitudes with anisotropic displacement parameters for all non-hydrogen atoms using Olex2 or SHELXL-2018/3 was employed.[71,72] All non-hydrogen atoms were refined anisotropically, while the hydrogen atoms were placed at calculated positions and further treated as riding on their parent atoms. Additional details on the crystal data, data collection and refinement are given in the Table S2.† Figures were prepared with *Mercury*.[73]

Synthesis of gold(III) complexes 1–7

Gold(III)–azole complexes **1–7** were synthesized by modification of the previously reported procedure for synthesis of gold(III) complexes with azine ligands.[39] The solution of 1.0 mmol of the corresponding azole (68.1 mg of im for **1**, 110.2 mg of ipim for **2**, 144.2 mg of phim for **3**, 344.8 mg of ctz for **4**, 444.7 mg of ecz for **5**, 387.7 mg of tcz for **6** and 349.3 mg of vcz for **7**) in 30.0 mL of ethanol was added slowly under stirring to the solution containing an equimolar amount of K[$AuCl_4$] (377.9 mg) in 5.0 mL of ethanol. The obtained solution was heated at 70 °C for 3 h in the absence of light. Gold(III)–azole complexes **1–7** were obtained from the mother ethanol solutions after their evaporation at room temperature for 3–4 days. In the case of complexes **3–5** and **7**, the yellow crystals suitable for single-crystal X-ray diffraction analysis were formed. These crystals were filtered off and dried in the dark at room temperature. Yield: 289.7 mg (78%) for **1**, 297.7 mg (72%) for **2**, 331.1 mg (74%) for **3**, 408.3 mg (63%) for **4**, 452.1 mg (66%) for **5**, 490.6 mg (71%) for **6** and 443.8 mg (68%) for **7**.

Anal. calcd for [$AuCl_3$(im)] (**1**) ($C_3H_4AuCl_3N_2$; MW = 371.40): C, 9.70; H, 1.09; N, 7.54. Found: C, 9.62; H, 1.01; N, 7.41%. ESI-HRMS (CH_3CN): m/z calcd for $[C_5H_7AuN_3]^{3+}$: 306.0305; found: 306.0299. IR (KBr, ν, cm^{-1}): 3130s (ν(N–H)), ~3000w ($\nu(C_{diazole}–H)$), 1636m, 1579m, 1548w, 1411w (ν(C=C) and ν(C=N)), 758m, 737m, 617m ($\gamma(C_{diazole}–H)$). ^{1}H NMR (200 MHz, DMSO-d_6): δ = 8.74 (d, J = 47.0 Hz, 1H, C2H), 7.48 (dd, J = 20.5, 19.2 Hz, 2H, C4H and C5H). UV-Vis ($CHCl_3$, λ_{max}, nm): 260 ($\varepsilon = 2.4 \times 10^3$ M^{-1} cm^{-1}). Λ_M (DMF): 26.3 Ω^{-1} cm^2 mol^{-1}.

Anal. calcd for [$AuCl_3$(ipim)] (**2**) ($C_6H_{10}AuCl_3N_2$; MW = 413.48): C, 17.43; H, 2.44; N, 6.77. Found: C, 17.25; H, 2.26; N, 6.57%. ESI-HRMS (CH_3CN): m/z calcd for $[C_8H_{13}AuN_3]^{3+}$: 348.0775; found: 348.0773. IR (KBr, ν, cm^{-1}): 3152m, 3133s ($\nu(C_{diazole}–H)$), 2978m, 2929w (ν(C–H)), 1606m, 1542m, 1523s, 1459m, 1373m (ν(C=C) and ν(C=N)), 826m, 818m, 748m, 650m, 631m ($\gamma(C_{diazole}–H)$). ^{1}H NMR (200 MHz, DMSO-d_6): δ = 8.73 (d, J = 1.3 Hz, 1H, C2H), 7.83 (dt, J = 12.4, 1.7 Hz, 1H, C4H), 7.48 (*m*, 1H, C5H), 4.70 (dq, J = 20.1, 6.8 Hz, 1H, C6H), 1.44 (q, J = 6.1 Hz, 6H, C7H and C8H). UV-Vis ($CHCl_3$, λ_{max}, nm): 315 ($\varepsilon = 1.7 \times 10^3$ M^{-1} cm^{-1}). Λ_M (DMF): 35.5 Ω^{-1} cm^2 mol^{-1}.

Anal. calcd for [$AuCl_3$(phim)] (**3**) ($C_9H_8AuCl_3N_2$; MW = 447.49): C, 24.16; H, 1.80; N, 6.26. Found: C, 24.08; H, 1.72; N, 6.34%. ESI-HRMS (CH_3CN): m/z calcd for $[C_{11}H_{11}AuN_3]^{3+}$: 382.0618; found: 3823.0610. IR (KBr, ν, cm^{-1}): 3158m, 3131m, 3061w ($\nu(C_{diazole}–H)$ and $\nu(C_{ar}–H)$), 1594m, 1538m, 1518s, 1492m, 1460m ($\nu(C_{ar}=C_{ar})$ and ν(C=N)), 828m, 761s, 749m, 737m, 692m ($\gamma(C_{ar}–H)$ and $\gamma(C_{diazole}–H)$). ^{1}H NMR (200 MHz, DMSO-d_6): δ = 9.25 (s, 1H, C2H), 8.23 (s, 1H, C4H), 7.66 ppm (m, 6H, C5H, C7H–C11H). UV-Vis ($CHCl_3$, λ_{max}, nm): 299 ($\varepsilon = 1.7 \times 10^3$ M^{-1} cm^{-1}). Λ_M (DMF): 18.08 Ω^{-1} cm^2 mol^{-1}.

Anal. calcd for [$AuCl_3$(ctz)] (**4**) ($C_{22}H_{17}AuCl_4N_2$; MW = 648.16): C, 40.77; H, 2.64; N, 4.32. Found: C, 40.59; H, 2.42; N, 4.34%. ESI-HRMS (CH_3CN): no signal observed. IR (cm^{-1}, KBr): 3126w, 3101w ($\nu(C_{ar}–H)$ and $\nu(C_{diazole}–H)$), 2930w (ν(C–H)), 1508w, 1465w, 1446m, 1432w ($\nu(C_{ar}=C_{ar})$ and ν(C=N)), 756m, 747m, 704m, 679m, 669m ($\gamma(C_{ar}–H)$) and ($\gamma(C_{diazole}–H)$), 638w (ν(C–Cl)). ^{1}H NMR (500 MHz, $CDCl_3$): δ = 8.41 (t, J = 1.5 Hz, 1H, C2H), 7.66 (m, 1H, C8H), 7.51 (dd, J = 7.9, 1.4 Hz, 1H, C9H), 7.43 (m, 7H, C10H, C14H, C15H, C16H, C20H, C21H, C22H), 7.32 (m, 1H, C4H), 7.10 (m, 4H, C13H, C17H, C19H, C23H), 6.99 (dd, J = 3.3, 1.6 Hz, 1H, C5H), 6.98 ppm (dd, J = 8.0, 1.4 Hz, 1H, C11H). UV-Vis ($CHCl_3$, λ_{max}, nm): 301 ($\varepsilon = 2.0 \times 10^3$ M^{-1} cm^{-1}). Λ_M (DMF): 7.89 Ω^{-1} cm^2 mol^{-1}.

Anal. calcd for [$AuCl_3$(ecz)] (**5**) ($C_{18}H_{15}AuCl_6N_2O$; MW = 684.99): C, 31.56; H, 2.21; N, 4.09. Found: C, 31.67; H, 1.96; N, 4.05%. ESI-HRMS (CH_3CN): m/z calcd for $[C_{20}H_{18}AuCl_3N_3O]^+$: 618.0181; found: 618.0174. IR (KBr, ν, cm^{-1}): ~3100m ($\nu(C_{diazole}–H)$ and $\nu(C_{ar}–H)$), 2871w (ν(C–H)), 1590m, 1563w, 1543w, 1522m, 1491m, 1436w ($\nu(C_{ar}=C_{ar})$ and ν(C=N)), 1246w, 1223w ($\beta(C_{ar}–H)$ and $\beta(C_{diazole}–H)$), 1110s (ν(C–O)), 1093vs, 1044m, 1015m ($\nu(C_{ar}–Cl)$), 808m, 787m, 737w, 669w, 632w ($\gamma(C_{ar}–H)$) and ($\gamma(C_{diazole}–H)$). ^{1}H NMR (500 MHz, $CDCl_3$): δ = 8.36 (s, 1H, C2H), 7.59 (m, 1H, C10H), 7.48 (d, J = 1.9 Hz, 1H, C4H), 7.37 (dd, J = 8.4, 1.9 Hz, 1H, C5H), 7.35 (m, 1H, C13H), 7.33 (d, J = 1.8 Hz, 1H, C12H), 7.32 and 7.09 (m, 2H, C17H, C19H), 7.08 and 7.02 (m, 2H, C16H, C20H), 4.98 (dd, J = 7.8, 2.6 Hz, 1H, C7H), 4.52 (d, J = 11.7 Hz, 1H, C6H), 4.29 (dd, J = 14.4, 2.6 Hz, 1H, C6H), 4.21 (d, J = 11.7 Hz, 1H, C14H), 4.14 ppm (dd, J = 14.4, 7.8 Hz, 1H, C14H). UV-Vis ($CHCl_3$, λ_{max}, nm): 300 ($\varepsilon = 1.8 \times 10^3$ M^{-1} cm^{-1}). Λ_M (DMF): 14.34 Ω^{-1} cm^2 mol^{-1}.

Anal. calcd for [$AuCl_3$(tcz)] (**6**) ($C_{16}H_{13}AuCl_6N_2OS$; MW = 691.04): C, 27.81; H, 1.90; N, 4.05. Found: C, 27.91; H, 1.78; N, 4.08%. ESI-HRMS (CH_3CN): m/z calcd for $[C_{16}H_{13}AuCl_5N_2OS]^+$:

654.8827; found: 654.8813. IR (KBr, ν, cm^{-1}): 3182w, 3157w, 3139m, 3101w, 3090w ($\nu(C_{diazole}–H)$ and $\nu(C_{ar}–H)$), 2931w (ν(C–H)), 1589m, 1542m, 1521m, 1468m, 1440m ($\nu(C_{ar}=C_{ar})$ and ν(C=N)), 1244w, 1230w, 1213w ($\beta(C_{ar}–H)$ and $\beta(C_{diazole}–H)$), 1103vs, 1087s (ν(C–O)), 825m, 788m, 686w ($\gamma(C_{ar}–H)$), 748s (ν(C–S)), 637m (ν(C–Cl)). ^{1}H NMR (500 MHz, $CDCl_3$): δ = 8.32 (s, 1H, C2H), 7.58 (m, 1H, C10H), 7.48 (m, 1H, C12H), 7.37 (m, 2H, C13H, C17H), 7.14 (t, J = 7.2 Hz, 1H, C5H), 7.03 (t, J = 1.7 Hz, 1H, C16H), 6.77 (d, J = 5.7 Hz, 1H, C4H), 4.96 (dd, J = 8.2, 2.5 Hz, 1H, C7H), 4.49 (t, J = 12.2 Hz, 1H, C14H), 4.26 (m, 2H, C6H, C14H), 4.07 ppm (dd, J = 14.4, 8.2 Hz, 1H, C6H). UV-Vis ($CHCl_3$, λ_{max}, nm): 301 (2.0×10^3 M^{-1} cm^{-1}). Λ_M (DMF): 3.32 Ω^{-1} cm^2 mol^{-1}.

Anal. calcd for [$AuCl_3$(vcz)] (7) ($C_{16}H_{14}AuCl_3F_3N_5O$; MW = 652.64): C, 29.45; H, 2.16; N, 10.73. Found: C, 29.22; H, 1.98; N, 10.63%. ESI-HRMS (CH_3CN): m/z calcd for $[C_{16}H_{15}AuCl_3F_3N_5O]^+$: 651.9960; found: 651.9952. IR (KBr, ν, cm^{-1}): 3436br (ν(O–H)), 3145m, 3041w, 3016w, 3003w ($\nu(C_{triazole}–H)$ and $\nu(C_{ar}–H)$), 2986w, 2967w, 2942w (ν(C–H)), 1621s, 1589s, 1547s, 1500s, 1459m, 1405s ($\nu(C_{ar}=C_{ar})$ and ν(C=N)), 1273m (δ(O–H)), 1254w, 1214w ($\beta(C_{ar}–H)$ and $\beta(C_{triazole}–H)$), 1129vs (ν(C–F)), 1056m (ν(C–O)), 864m, 847m, 832w, 789w, 676w ($\gamma(C_{ar}–H)$) and ($\gamma(C_{triazole}–H)$), 578w ($\beta(C_{ar}–F)$). ^{1}H NMR (500 MHz, $CDCl_3$): δ = 9.11 (s, 1H, C18H), 9.08 (d, J = 2.3 Hz, 1H, C20H), 8.73 (s, 1H, C5H), 8.27 (s, 1H, C3H), 7.55 (td, J = 9.1, 6.5 Hz, 1H, C9H), 6.91 (m, 1H, C12H), 6.87 (dd, J = 9.2, 3.2 Hz, 1H, C10H), 6.84 (s, 1H, OH), 4.92 (d, J = 13.9 Hz, 1H, C6H), 4.33 (d, J = 13.9 Hz, 1H, C6H), 4.16 (q, J = 7.0 Hz, 1H, C14H), 1.13 ppm (d, J = 7.1 Hz, 3H, C15H). UV-Vis ($CHCl_3$, λ_{max}, nm): 305 (ε = 1.7×10^3 M^{-1} cm^{-1}). Λ_M (DMF): 3.84 Ω^{-1} cm^2 mol^{-1}.

For comparative purposes, all selected azoles were characterized by ^{1}H NMR, IR and UV-Vis spectroscopy and these data are provided in ESI.†

Antimicrobial properties: determination of minimum inhibitory concentrations (MIC)

MIC values were determined with microdilution assays, according to standardized methodology, commonly used in microbiology laboratories. Standardized methodology used in this study is recommended by the National Committee for Clinical Laboratory Standards (M07-A8) for bacteria and Standards of European Committee on Antimicrobial Susceptibility Testing (v 7.3.1: method for the determination of broth dilution minimum inhibitory concentrations of antifungal agents for yeasts) for *Candida* spp. For the assessment of the antimicrobial potential of tested compounds in this study pathogenic bacterial and fungal species were used. Bacterial test organisms included: *Escherichia coli* NCTC 9001, *Pseudomonas aeruginosa* NCTC 10332, *Pseudomonas aeruginosa* PA14, *P. aeruginosa* BK25H,[66] *Staphylococcus aureus* ATCC 25923, *Staphylococcus aureus* NCTC 6571, *Staphylococcus aureus* MRSA and *Candida* strains: *C. albicans* ATCC 10231, *C. parapsilosis* ATCC 22019, *C. glabrata* ATCC 2001, *C. krusei* ATCC 6258 and *C. auris* ATCC 21092. All tested compounds were first dissolved in DMSO, at a concentration of 50 mg mL^{-1}, which allowed to reach high concentrations in μg mL^{-1} for further dilutions. The highest concentration used was 200 mg mL^{-1}. The inoculums were 5×10^5 colony forming units, cfu mL^{-1}, for bacteria and 1×10^5 cfu mL^{-1} for fungal species. The MIC value was recorded as the lowest concentration that inhibited the growth after 24 h at 37 °C, using the Tecan Infinite 200 Pro multiplate reader (Tecan Group Ltd, Männedorf, Switzerland). Experiments were done in triplicate for each concentration and repeated at least two times per tested strain.

Microsporum canis was obtained from skin swab of a dog in veterinary laboratory VetLab Ltd, Belgrade, Serbia. Fungi was isolated and propagated on Sabouraud agar plates. Experiment was carried in 24-well plates. Fresh Sabouraud liquid medium was prepared and after colling at 50 °C, 3 mL of medium was aliquoted and mixed with compounds or ligands and poured in wells of 24-well plate. Final concentrations of compounds and ligands were 25 and 50 μg mL^{-1}. After colling at room temperature for 1 h, *M. canis* was added using sterile toothpicks. Plates were incubated at room temperature for 7 days and wells were observed after 4 and 7 days. Medium with *M. canis*, as well as medium without fungi, served as positive and negative controls.

Cytotoxicity assay

Cytotoxicity of the gold(III) complexes and the corresponding azole ligands was determined as antiproliferative effect on human fibroblast MRC-5 (obtained from ATCC), as described previously.[74]

Ergosterol analysis

Ergosterol levels in untreated cultures of *C. albicans* ATCC 10231 and cultures treated with 0.5 × MIC concentration of azoles im, ipim, phim, and their complexes **1–3**, respectively, were assessed after 18 h incubation at 37 °C on the rotary shaker (180 rpm) following the procedure.[75] Using Ultrospec 3300pro 573 (Amersham Biosciences, Amersham, UK), spectrophotometer ergosterol levels (concentrations) were determined by scanning absorbance between 240 and 300 nm.

Anti-quorum sensing (QS) activity

Violacein and prodigiosin inhibition. For the assessment of the violacein production, the *Chromobacterium violaceum* CV026 strain was used.[76] This strain was cultivated overnight at 30 °C and 180 rpm. Into semi-solid LB agar (0.3%, w/v, 5 mL), 50 μL of an overnight culture of *C. violaceum* CV026 was seeded and that was supplemented with *N*-hexanoyl-L-homoserine lactone (Sigma, Germany) to a final concentration of 5 μM and it was poured over the surface of LB agar plates. After solidification, the sterile discs were placed into the surface of plates and the tested compounds added in appropriate concentrations. Petri dishes were incubated at 30 °C in upright position overnight.

For the prodigiosin production, *Serratia marcescens* ATCC 27117 was used. The methodology is the same as for the

C. violaceum CV026 beside adding external autoinducer, because this is a wild type strain naturally capable of its production.[77] Inhibition of violacein and prodigiosin production was defined as the presence of blurry white hallows around discs containing active compound, measured in mm.

Pyocyanin inhibition. The assay used for determination of pyocyanin production was previously published in 2013 by O'Loughlin and co-workers[78] with minor modifications. *Pseudomonas aeruginosa* PA14 strain was cultivated overnight, and that culture was subcultured 1 : 1000 in 5 mL fresh LB medium. Gold(III)–azole compounds where assayed in subinhibitory concentration of 50 and 20 μg mL^{-1}, the incubation period was 20 h at 37 °C on a rotary shaker 180 rpm. OD_{600} was measured for full cultures, and cells were separated from culture fluids by centrifugation, 13 000 rpm for 15 min. OD_{695} of supernatants were measured on spectrophotometer Ultrospec 3300pro 573 (Amersham Biosciences, USA). Values of OD_{695} were normalized per cell density.

In vitro cell infections

In vitro cell infections assay was performed according to O'Loughlin *et al.* with minor modifications.[78] Activity of compounds **5** and **6** and the corresponding ligands ecz and tcz azoles, respectively, was evaluated at concentration 2.5 and 5 μg mL^{-1}. Clinical strain *P. aeruginosa* BK25H was obtained from our laboratory collection.[66] Human lung carcinoma cells (A549) were obtained from the American Type Culture Collection (ATCC; Manassas, Virginia, USA). Cells were maintained as monolayer cultures in RPMI-1640 supplemented with 10% (v/v) FBS (all from Sigma). Cells were grown in a humidified atmosphere of 95% air and 5% CO_2 at 37 °C. Human A549 cells were grown in culture flasks (Sarstedt, Nümbrecht, Germany). Before infection, the A549 cells were treated with trypsin–EDTA (Sigma), split, counted, and aliquoted into 96-well plates at 100 000 mammalian cells per well. Cells were grown for 20 h and then washed 3 times with PBS (Sigma) before bacterial suspension adjusted to final OD_{600} of 0.02 in 100 μL of RPMI containing 10 μg mL^{-1} propidium iodide (PI; Sigma) and tested compounds were added. PI fluorescence was measured after 10 h (excitation/emission (nm): 535/617) using Tecan Infinite M200 pro plate reader. Appropriate controls such as bacteria in the absence of A549 cells, cells with DMSO as well as cells without addition of bacterial suspension and compounds were included in experiment. The cytotoxicity was calculated according to formula:

$$\mathrm{Cyt}(\%) = (F_{\mathrm{bact}}/F_{\mathrm{det}}) \times 100$$

where F_{bact} represents cytotoxicity obtained in the presence of bacteria with compounds and F_{det} represents fluorescence of noninfected cells lysed with 0.1% Triton-X100.

Statistical analysis

The results were expressed as mean values ± standard deviation (SD) and analyzed using Student's *t*-test at a threshold level of $p = 0.5$. This analysis was carried out using SPSS 20 (SPSS Inc., Chicago, IL) software.

Conclusions

All synthesized [$AuCl_3$(azole)] complexes, where azole is imidazole (**1**), 1-isopropylimidazole (**2**), 1-phenylimidazole (**3**), clotrimazole (**4**), econazole (**5**), tioconazole (**6**) and voriconazole (**7**) are mononuclear coordination compounds, in which the azole ligand is monodentately coordinated to the Au(III) ion *via* the imidazole or triazole nitrogen atom, while the remaining coordination sites are occupied by chlorido ligands resulting in a square-planar arrangement around the metal center. This work represents a significant contribution to the structural knowledge of gold(III) compounds with four crystal structures of gold(III)–azole complexes which include one model azole (phim; complex **3**) and three antifungal azoles (complexes **4**, **5** and **7**). For econazole (complex **5**), we report the first ever crystal structure of a metal complex. The antimicrobial potential of these complexes was assessed *in vitro* against five fungal and seven bacterial species, common and emerging human and animal pathogens. The influence of the coordinated Au(III) ion on the antimicrobial potential of the investigated complexes was determined by comparing their activities with those for uncoordinated inactive and antifungal azoles. We found that complexation of biologically inactive imidazole, 1-isopropylimidazole and 1-phenylimidazole with an Au(III) species resulted in gold(III) complexes **1–3** with moderate antimicrobial activity against the investigated strains and low cytotoxicity to human normal lung fibroblast cell line (MRC-5). Moreover, the gold(III) complexes **4–7** with clinically used antifungal agents clotrimazole, econazole, tioconazole and voriconazole showed higher antimicrobial effectiveness than the corresponding azoles in most cases, with the best improvement obtained after auration of tioconazole (**6**) and voriconazole (**7**). Also, the gold(III) complexes **1–3** significantly decreased ergosterol levels in *C. albicans*, compared to the respective uncoordinated non-antifungal imidazole and its two derivatives 1-isopropylimidazole and 1-phenylimidazole, confirming undoubtedly that the presence of the Au(III) ion in these complexes affects ergosterol biosynthesis and its incorporation into the cell membrane of the investigated strain. The comparative study of the quorum sensing inhibitory potential of the selected azoles and the corresponding gold(III) complexes **1–7** showed that these complexes significantly inhibited bacterial pigment pyocyanin production. In particular, complexes **5** and **6** were the most potent inhibitors of pyocyanin production and were active even at concentrations as low as 2 μg mL^{-1} (2.9 μM). Apart from econazole and tioconazole, the other investigated azoles showed no detectable activity under the same experimental conditions. Overall, we have demonstrated that the strategy based on the coordination of existing azole-based drugs to the Au(III) ion could be successfully used in the development of improved antifungal or novel anti-virulent therapeutic agents that attenuate virulence of pathogens without

pronounced effects on growth, providing a lower risk for the development of resistance.

Conflicts of interest

The authors declare no conflicts of interest.

Acknowledgements

This research has been financially supported by the Ministry of Education, Science and Technological Development of the Republic of Serbia (Agreement No. 451-03-68/2022-14/200042 and 451-03-68/2022-14/200122) and by the Slovenian Research Agency (grant P1-0175). The EN→FIST Centre of Excellence, Trg OF 13, SI-1000 Ljubljana, Slovenia, is acknowledged for the use of the SuperNova diffractometer. This research has also received funding from the Serbian Academy of Sciences and Arts under strategic projects programme – grant agreement no. 01-2019-F65 and project of this institution no. F128. N. Lj. S. is gratefully acknowledged to the Ministry of Education, Science and Sport of the Republic of Slovenia for awarding the nine months Mobility Grant (CMEPIUS) at the University of Ljubljana, Faculty of Chemistry and Chemical Technology.

Notes and references

1 B. Đ. Glišić and M. I. Djuran, *Dalton Trans.*, 2014, **43**, 5950–5969.
2 A. Frei, J. Zuegg, A. G. Elliott, M. Baker, S. Braese, C. Brown, F. Chen, C. G. Dowson, G. Dujardin, N. Jung, A. P. King, A. M. Mansour, M. Massi, J. Moat, H. A. Mohamed, A. K. Renfrew, P. J. Rutledge, P. J. Sadler, M. H. Todd, C. E. Willans, J. J. Wilson, M. A. Cooper and M. A. T. Blaskovich, *Chem. Sci.*, 2020, **11**, 2627–2639.
3 M. Rai, S. D. Deshmukh, A. P. Ingle, I. R. Gupta, M. Galdiero and S. Galdiero, *Crit. Rev. Microbiol.*, 2016, **42**, 46–56.
4 Y. C. Ong, S. Roy, P. C. Andrews and G. Gasser, *Chem. Rev.*, 2019, **119**, 730–796.
5 U. Ndagi, N. Mhlongo and M. E. Soliman, *Drug Des., Dev. Ther.*, 2017, **11**, 599–616.
6 S. J. Berners-Price and A. Filipovska, *Metallomics*, 2011, **3**, 863–873.
7 M. Alda, *Mol. Psychiatry*, 2015, **20**, 661–670.
8 J. A. R. Salvador, S. A. C. Figueiredo, R. M. A. Pinto and S. M. Silvestre, *Future Med. Chem.*, 2012, **4**, 1495–1523.
9 C. N. Morrison, K. E. Prosser, R. W. Stokes, A. Cordes, N. Metzler-Nolte and S. M. Cohen, *Chem. Sci.*, 2020, **11**, 1216–1225.
10 A. Frei, *Antibiotics*, 2020, **9**, 90.
11 Z. Huaizhi and N. Yuantao, *Gold Bull.*, 2001, **34**, 24–29.
12 N. P. Wiederhold, T. F. Patterson, A. Srinivasan, A. K. Chaturvedi, A. W. Fothergill, F. L. Wormley, A. K. Ramasubramanian and J. L. Lopez-Ribot, *Virulence*, 2017, **8**, 138–142.
13 G. Roymahapatra, S. M. Mandal, W. F. Porto, T. Samanta, S. Giri, J. Dinda, O. L. Franco and P. K. Chattaraj, *Curr. Med. Chem.*, 2012, **19**, 4184–4193.
14 T. Samanta, G. Roymahapatra, W. F. Porto, S. Seth, S. Ghorai, S. Saha, J. Sengupta, O. L. Franco, J. Dinda and S. M. Mandal, *PLoS One*, 2013, **8**, e58346.
15 D. G. Brown, T. L. May-Dracka, M. M. Gagnon and R. Tommasi, *J. Med. Chem.*, 2014, **57**, 10144–10161.
16 M. B. Harbut, C. Vilchèze, X. Luo, M. E. Hensler, H. Guo, B. Yang, A. K. Chatterjee, V. Nizet, W. R. Jacobs, P. G. Schultz and F. Wang, *Proc. Natl. Acad. Sci. U. S. A.*, 2015, **112**, 4453–4458.
17 C. Schmidt, B. Karge, R. Misgeld, A. Prokop, R. Franke, M. Brönstrup and I. Ott, *Chem. – Eur. J.*, 2017, **23**, 1869–1880.
18 P. Chakraborty, D. Oosterhuis, R. Bonsignore, A. Casini, P. Olinga and D.-J. Scheffers, *ChemMedChem*, 2021, **16**, 1–12.
19 A. P. Taylor, R. P. Robinson, Y. M. Fobian, D. C. Blakemore, L. H. Jones and O. Fadeyi, *Org. Biomol. Chem.*, 2016, **14**, 6611–6637.
20 R. Tandon, I. Singh, V. Luxami, N. Tandon and K. Paul, *Chem. Rec.*, 2019, **19**, 362–393.
21 T. J. Gintjee, M. A. Donnelley and G. R. Thompson III, *J. Fungi*, 2020, **6**, 28.
22 R. Van Daele, I. Spriet, J. Wauters, J. Maertens, T. Mercier, S. Van Hecke and R. Brüggemann, *Med. Mycol.*, 2019, **57**, S328–S343.
23 J. R. Perfect, *Nat. Rev. Drug Discovery*, 2017, **16**, 603–616.
24 G. R. Thompson, J. Cadena and T. F. Patterson, *Clin. Chest Med.*, 2009, **30**, 203–215.
25 D. Li, X. She and R. Calderone, *FEMS Yeast Res.*, 2020, **20**, foaa023.
26 P. Dandawate, S. Padhye, R. Schobert and B. Biersack, *Expert Opin. Drug Discovery*, 2019, **14**, 563–576.
27 R. A. Sánchez-Delgado, M. Navarro, K. Lazardi, R. Atencio, M. Capparelli, F. Vargas, J. A. Urbina, A. Bouillez, A. F. Noels and D. Masi, *Inorg. Chim. Acta*, 1998, **275–276**, 528–540.
28 A. W. Addison, T. N. Rao, J. Reedijk, J. van Rijn and G. C. Verschoor, *J. Chem. Soc., Dalton Trans.*, 1984, 1349–1356.
29 T. D. Cyr, B. A. Dawson, G. A. Neville and H. F. Shurvell, *J. Pharm. Biomed. Anal.*, 1996, **14**, 247–255.
30 N. L. Calvo, V. A. Alvarez, M. C. Lamas and D. Leonardi, *J. Pharm. Anal.*, 2019, **9**, 40–48.
31 W. J. Geary, *Coord. Chem. Rev.*, 1971, **7**, 81–122.
32 I. Ali, W. A. Wani and K. Saleem, *Synth. React. Inorg., Met.-Org., Nano-Met. Chem.*, 2013, **43**, 1162–1170.
33 K. Esumi, M. Nawa, N. Aihara and K. Usui, *New J. Chem.*, 1998, **22**, 719–720.
34 N. Pantelić, B. B. Zmejkovski, J. Trifunović-Macedoljan, A. Savić, D. Stanković, A. Damjanović, Z. Juranić, G. N. Kaluđerović and T. J. Sabo, *J. Inorg. Biochem.*, 2013, **128**, 146–153.

35 N. Pantelić, T. P. Stanojković, B. B. Zmejkovski, T. J. Sabo and G. N. Kaluđerović, *Eur. J. Med. Chem.*, 2015, **90**, 766–774.
36 J. Kljun, A. J. Scott, T. Lanišnik Rižner, J. Keiser and I. Turel, *Organometallics*, 2014, **33**, 1594–1601.
37 J. Kujawski, K. Czaja, E. Jodłowska, K. Dettlaff, M. Politańska, J. Żwawiak, R. Kujawski, T. Ratajczak, M. K. Chmielewski and M. K. Bernard, *J. Mol. Struct.*, 2016, **1119**, 250–258.
38 Y.-H. Ou, R.-K. Du, S.-P. Zhang, Y. Ling, S. Li, C.-J. Zhao, W.-Z. Zhang and L. Zhang, *J. Mol. Struct.*, 2020, **1215**, 128229.
39 B. Warżajtis, B. Đ. Glišić, N. S. Radulović, U. Rychlewska and M. I. Djuran, *Polyhedron*, 2014, **79**, 221–228.
40 E. Lefler and D. A. Stevens, *Antimicrob. Agents Chemother.*, 1984, **25**, 450–454.
41 B. Warżajtis, B. Đ. Glišić, N. D. Savić, A. Pavić, S. Vojnovic, A. Veselinović, J. Nikodinovic-Runic, U. Rychlewska and M. I. Djuran, *Dalton Trans.*, 2017, **46**, 2594–2608.
42 B. O'Brien, S. Chaturvedi and V. Chaturvedi, *Antimicrob. Agents Chemother.*, 2020, **64**, e02195–e02119.
43 C. I. Aneke, D. Otranto and C. Cafarchia, *J. Fungi*, 2018, **4**, 107.
44 K. Sahni, S. Singh and S. Dogra, *Indian Dermatol. Online J.*, 2018, **9**, 149–158.
45 B. E. Elewski, *Clin. Microbiol. Rev.*, 1998, **11**, 415–429.
46 S. R. Lockhart, K. A. Etienne, S. Vallabhaneni, J. Farooqi, A. Chowdhary, N. P. Govender, A. L. Colombo, B. Calvo, C. A. Cuomo, C. A. Desjardins, E. L. Berkow, M. Castanheira, R. E. Magobo, K. Jabeen, R. J. Asghar, J. F. Meis, B. Jackson, T. Chiller and A. P. Litvintseva, *Clin. Infect. Dis.*, 2017, **64**, 134–140.
47 J. Osei Sekyere, *MicrobiologyOpen*, 2018, **7**, e00578–e00578.
48 N. D. Savić, D. R. Milivojevic, B. Đ. Glišić, T. Ilic-Tomic, J. Veselinovic, A. Pavic, B. Vasiljevic, J. Nikodinovic-Runic and M. I. Djuran, *RSC Adv.*, 2016, **6**, 13193–13206.
49 E. R. T. Tiekink, *Gold Bull.*, 2003, **36**, 117–124.
50 A. G. Warrilow, J. E. Parker, D. E. Kelly and S. L. Kelly, *Antimicrob. Agents Chemother.*, 2013, **57**, 1352–1360.
51 B. A. Arthington-Skaggs, D. W. Warnock and C. J. Morrison, *Antimicrob. Agents Chemother.*, 2000, **44**, 2081–2085.
52 K. I. Teixeira, P. V. Araújo, R. D. Sinisterra and M. E. Cortés, *Braz. J. Microbiol.*, 2012, **43**, 810–818.
53 S. Sari, A. Avci, E. Koçak, D. Kart, S. Sabuncuoğlu, İ. S. Doğan, Z. Özdemir, İ. Bozbey, A. Karakurt, S. Saraç and S. Dalkara, *Drug Dev. Res.*, 2020, **81**, 1026–1036.
54 M. Alsterholm, N. Karami and J. Faergemann, *Acta Derm.-Venereol.*, 2010, **90**, 239–245.
55 S.-M. Frosini and R. Bond, *Antibiotics*, 2017, **6**, 29.
56 R. N. Jones, M. J. Bale, D. Hoban and M. E. Erwin, *Diagn. Microbiol. Infect. Dis.*, 1993, **17**, 45–51.
57 S. Khabnadideh, Z. Rezaei, A. Khalafi-Nezhad, R. Bahrinajafi, R. Mohamadi and A. A. Farrokhroz, *Bioorg. Med. Chem. Lett.*, 2003, **13**, 2863–2865.
58 A. K. Jain, V. Ravichandran, M. Sisodiya and R. K. Agrawal, *Asian Pac. J. Trop. Med.*, 2010, **3**, 471–474.
59 X.-Y. Sun, M.-Y. Liu, C.-Y. Zhong, G.-L. Zheng, M.-Y. Lv, B.-T. Jing, C.-Y. Pan and X. Wang, *J. Braz. Chem. Soc.*, 2018, **29**, 701–707.
60 B. Đ. Glišić, N. D. Savić, B. Warżajtis, L. Djokic, T. Ilic-Tomic, M. Antić, S. Radenković, J. Nikodinovic-Runic, U. Rychlewska and M. I. Djuran, *MedChemComm*, 2016, **7**, 1356–1366.
61 S. T. Rutherford and B. L. Bassler, *Cold Spring Harbor Perspect. Med.*, 2012, **2**, a012427.
62 P. Krzyżek, *Front. Microbiol.*, 2019, **10**, 2473.
63 T. Defoirdt, *Trends Microbiol.*, 2018, **26**, 313–328.
64 X. Chen, L. Zhang, M. Zhang, H. Liu, P. Lu and K. Lin, *Expert Opin. Ther. Pat.*, 2018, **28**, 849–865.
65 G. W. Lau, H. Ran, F. Kong, D. J. Hassett and D. Mavrodi, *Infect. Immun.*, 2004, **72**, 4275–4278.
66 D. Milivojevic, N. Šumonja, S. Medić, A. Pavic, I. Moric, B. Vasiljevic, L. Senerovic and J. Nikodinovic-Runic, *Pathog. Dis.*, 2018, **76**, fty041.
67 P. N. Jimenez, G. Koch, J. A. Thompson, K. B. Xavier, R. H. Cool and W. J. Quax, *Microbiol. Mol. Biol. Rev.*, 2012, **76**, 46–65.
68 K. Gałczyńska, K. Kurdziel, W. Adamus-Białek, S. Wąsik, K. Szary, M. Drabik, A. Węgierek-Ciuk, A. Lankoff and M. Arabski, *Acta Biochim. Pol.*, 2015, **62**, 739–745.
69 R. Frei, A. S. Breitbach and H. E. Blackwell, *Angew. Chem., Int. Ed.*, 2012, **51**, 5226–5229.
70 Oxford Diffraction Ltd, *CrysAlis PRO*, Yarnton, Oxfordshire, England, 2011.
71 O. V. Dolomanov, L. J. Bourhis, R. J. Gildea, J. A. K. Howard and H. Puschmann, *J. Appl. Crystallogr.*, 2009, **42**, 339–341.
72 G. M. Sheldrick, *Shelxl 2018/3*, University of Göttingen, Germany, 2018.
73 C. F. Macrae, P. R. Edgington, P. McCabe, E. Pidcock, G. P. Shields, R. Taylor, M. Towler and J. Van De Streek, *J. Appl. Crystallogr.*, 2006, **39**, 453–457.
74 M. B. Hansen, S. E. Nielsen and K. Berg, *J. Immunol. Methods*, 1989, **119**, 203.
75 B. A. Arthington-Skaggs, H. Jradi, T. Desai and C. J. Morrison, *J. Clin. Microbiol.*, 1999, **39**, 3332–3337.
76 K. H. McClean, M. K. Winson, L. Fish, A. Taylor, S. R. Chhabra, M. Camara, M. Daykin, J. H. Lamb, S. Swift, B. W. Bycroft, G. S. A. B. Stewart and P. Williams, *Microbiology*, 1997, **143**, 3703–3711.
77 I. Aleksić, S. Šegan, F. Andrić, M. Zlatović, I. Moric, D. M. Opsenica and L. Senerovic, *ACS Chem. Biol.*, 2017, **12**, 1425–1434.
78 C. T. O'Loughlin, L. C. Miller, A. Siryaporn, K. Drescher, M. F. Semmelhack and B. L. Bassler, *Proc. Natl. Acad. Sci. U. S. A.*, 2013, **110**, 17981–17986.